Proceedings of the Research Institute of Atmospherics,
Nagoya University, vol. 29 (1982) —Technical Report—

AN OBSERVATION SYSTEM OF INTERPLANETARY SCINTILLATION AT UHF

Masayoshi Kojima, Yoshio Ishida, Kazuo Maruyama
and
Takakiyo Kakinuma

Abstract

The paper describes the observation system of the interplanetary scintillation at UHF. General views of the antenna, the receiver system, the phase-gain calibration system and the data acquisition system are given.

1. IPS observations at UHF

IPS observations at a frequency of 69 MHz (VHF) have been conducted since 1971 at three stations (Toyokawa, Fuji and Sugadaira) as shown in Figure 1. Construction of a new system for the IPS observations at a frequency of 327 MHz (UHF) was started in 1977, and at the present time is almost completed.

As the line-of-sight approaches the sun, the degree of scintillation increases in proportion to the increase of electron density fluctuation, but finally it saturates and begins to decrease rapidly because of the strengthening of the radio scattering. This saturation occurs at a distance of 0.5 AU from the sun for 69 MHz, while this occurs in a region of as near as 0.2 AU for 327 MHz. Thus we can observe the solar wind over a wide range of radial distances

from 0.1 to 1 AU with two observation systems at VHF and UHF.

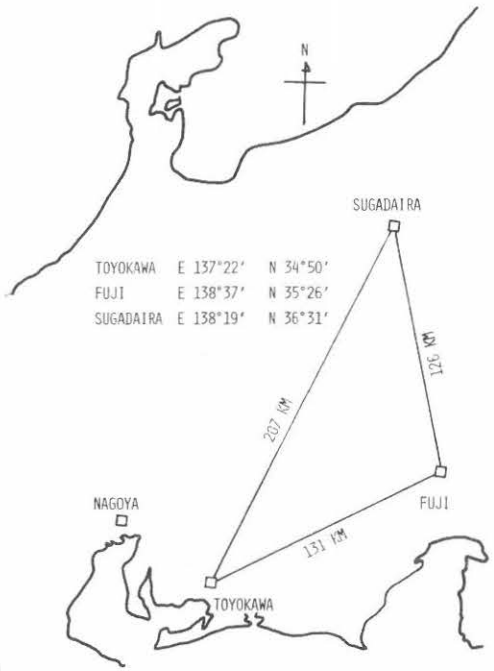

Fig. 1. Geometrical arrangement of three stations.

IPS observations at VHF are frequently interrupted by solar radio bursts, especially by high-intensity noise storms. However noise storms above 300 MHz rarely occurs, and it is expected that IPS observations at UHF will afford more oppotunities to detect interplanetary disturbances related to solar activities.

As the antennas of VHF and UHF are located at the same site, we can make simultaneous observations at two different frequencies. The dual frequency observations will offer new information about the solar wind plasma such as details about large density gradients in the solar wind which are too large to produce intensity scintillation (Gapper and Hewish, 1981).

2. General design

The antenna is an asymmetric parabolic cylinder similar to the telescopes at Bologna, Italy (Braccesi and Ceccarelli, 1962) and at Ootacamund, India (Swarup et al., 1971). The long axis of the cylinder is parallel to the east-west direction as shown in Figure 2. Tracking of a radio source is made by mechanical rotation of the antenna in the N-S direction and by electrical beam scanning with a phased array in the E-W direction. The receiver has a phase-gain calibration system. Two remote stations (Fuji and Sugadaira) are connected to the host station (Toyokawa) with public telephone lines for data acquisition. The observation system is automatically controlled with a minicomputer and two microprocessors.

3. The antenna system

3.1. The antenna

The antenna is an asymmetric parabolic cylinder which has a width of 20 m in the N-S direction and a length of 100 m in the E-W direction. The focal length is 10 m (Figure 2). The feed system including preamplifiers and phase shifters is placed near the focal line, but this asymmetric structure allows the feed system to be lowered to ground level for easy maintenance (Braccesi and Ceccarelli, 1962). The reflecting surface is made of 0.28 mmϕ stainless steel wires stretched at 3 cm spacing through five parabolic frames which are placed at 25 m intervals in the E-W direction. Each of the stainless steel wires is pulled by a spring. Total tension imposed on the end frames is counteracted by wire ropes tied to anchor bases as shown in Figure 2. The cylinder is illuminated by a corner reflector energized by a total of 192 half-wave dipoles. A corner angle is 90° and dipoles are placed at a distance of 0.6 wave-length from the apex.

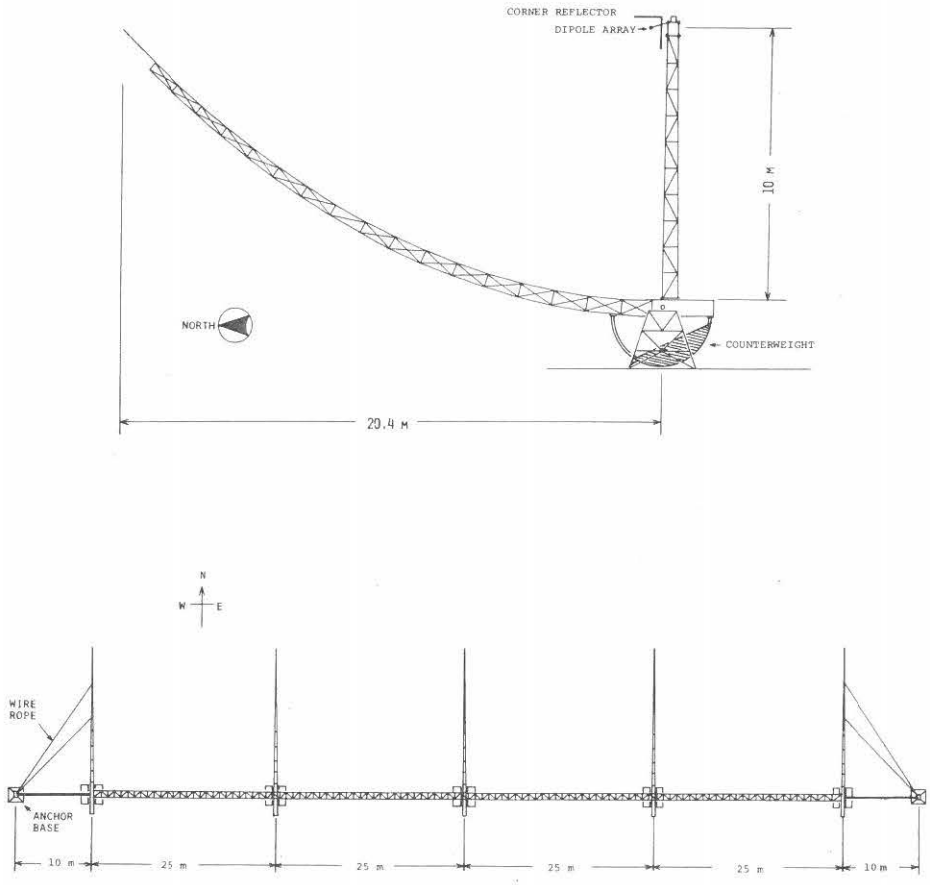

Fig. 2. The antenna structure and the arrangement at Fuji.

Surface accuracy of the antenna was calculated by measuring the angles of elevation and azimuth of marked points on the parabolic frame with two transists placed at a distance parallel to the frame (Figure 3). Average surface accuracy of five frames is 26 mm (rms)

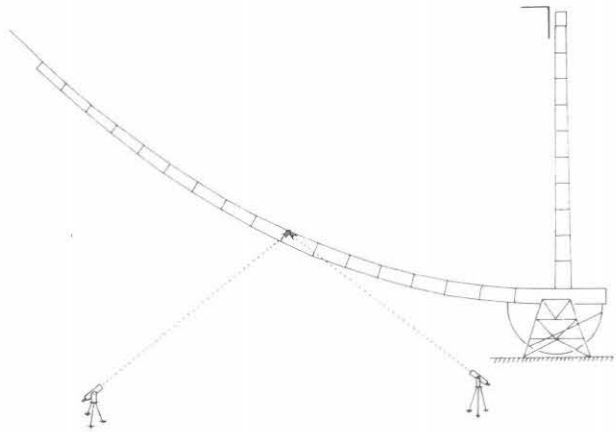

Fig. 3. Measurement of the surface accuracy with two transits.

As the antenna site at Fuji is situated in a national park, construction height is severely limited to 13 m. This made limitation on the antenna design and the position of the pivot shaft of the frame is shifted to the edge of the frame as shown in Figure 4. The Sugadaira antenna shown in Figure 5 is built on the north slope of the mountain.

3.2. The feed system

The dipole array along the focal line consists of 192 elements of the half-wave dipole which are spaced 0.56 wave-length apart. Outputs of two adjoining dipoles are combined and amplified with a low-noise preamplifier followed by a phase shifter. Phase controlled outputs of 96 phase shifters are combined with the X-mas tree branching system as shown in Figure 6. The feed system is constructed with coaxial cable (5D2W) and hybrid combiners. The total number of 96 preamplifiers and phase shifters was decided upon for financial reasons. Therefore the phased array is controlled by phase shifters spaced 0.56×2 wave-length apart, but the decrease of the antenna gain is as small as 1 db at a scan angle of $\pm 15°$.

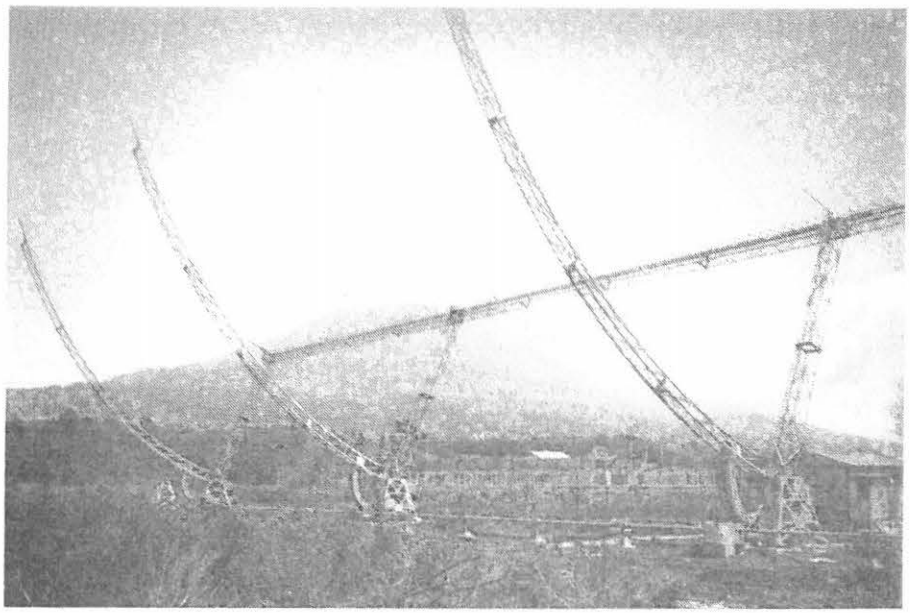

Fig. 4. UHF antenna and Mt. Fuji. VHF antenna is seen between them.

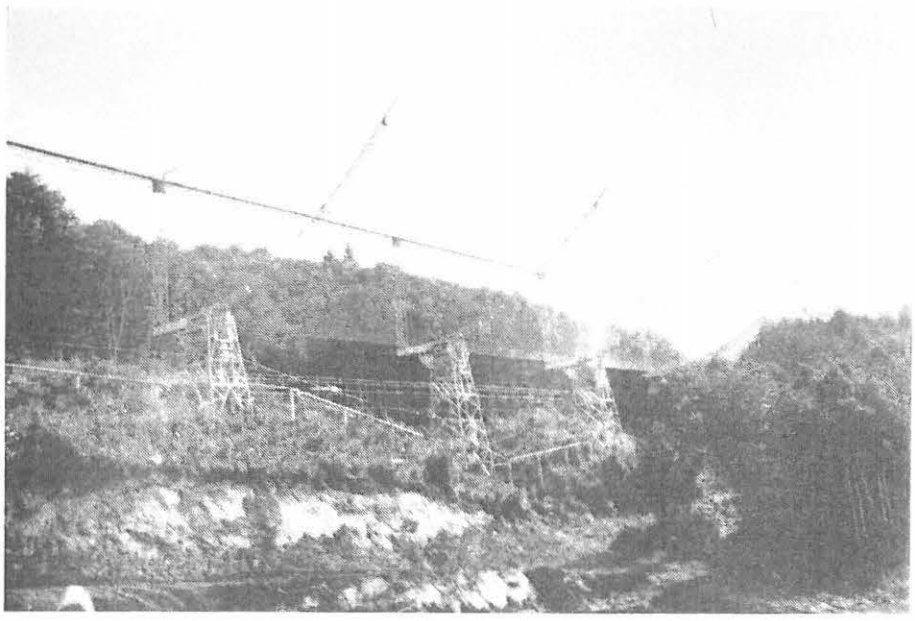

Fig. 5. UHF antenna at Sugadaira.

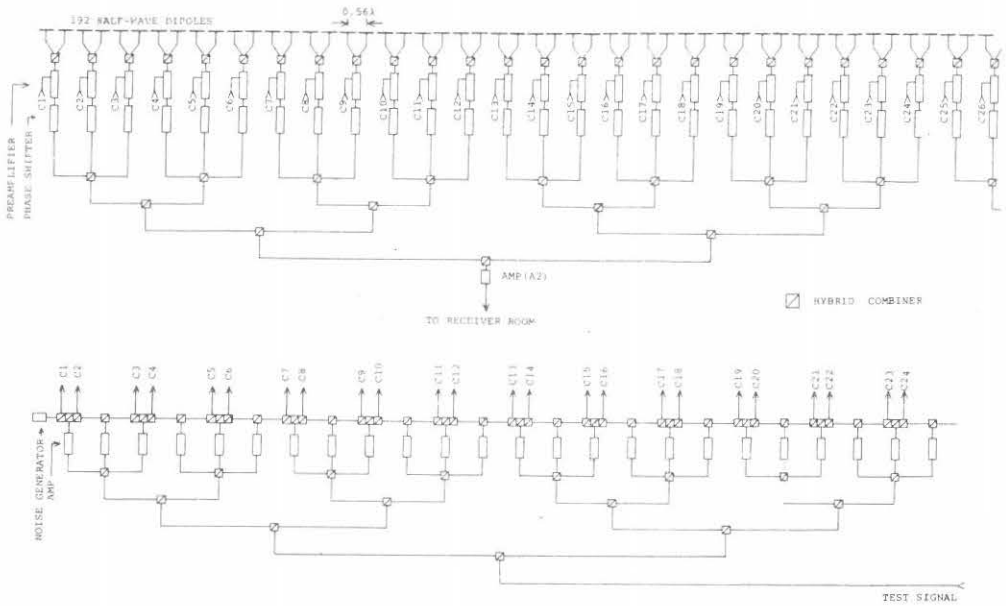

Fig. 6. A part of the feed system. The lower is the branching system of test signal for the calibration.

3.3. The dipole feed

A half-wave dipole is connected to a balun and the impedance matching between the dipole and the feed line (50Ω) is made by a parallel stub line (Figures 7 and 8).

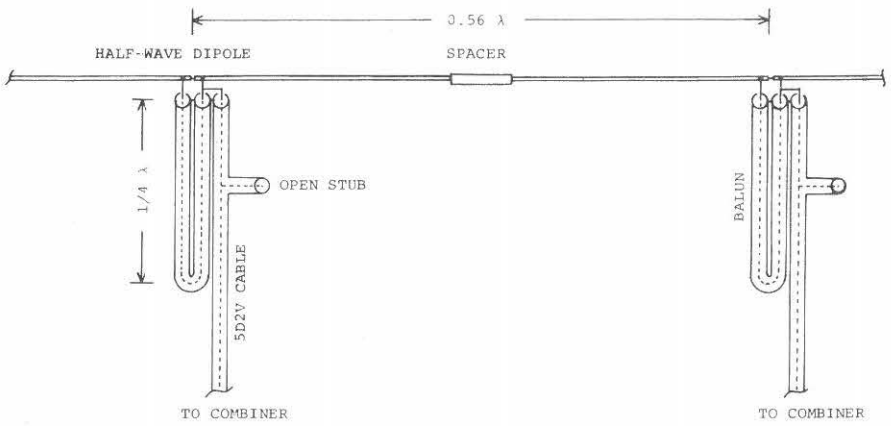

Fig. 7. Dipole feed structure.

Fig. 8. Installation of dipoles.

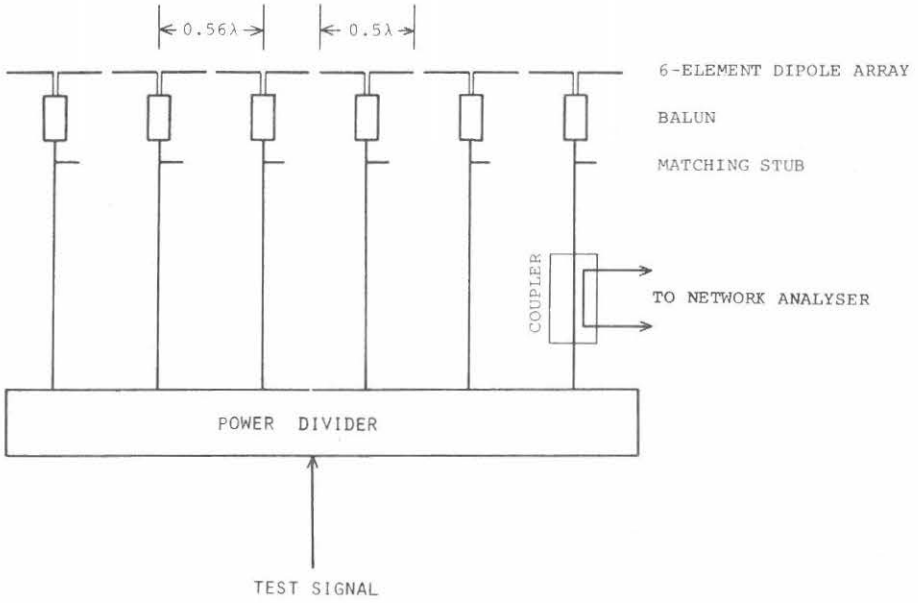

Fig. 9. Measurement of the active impedance of the 6-element array.

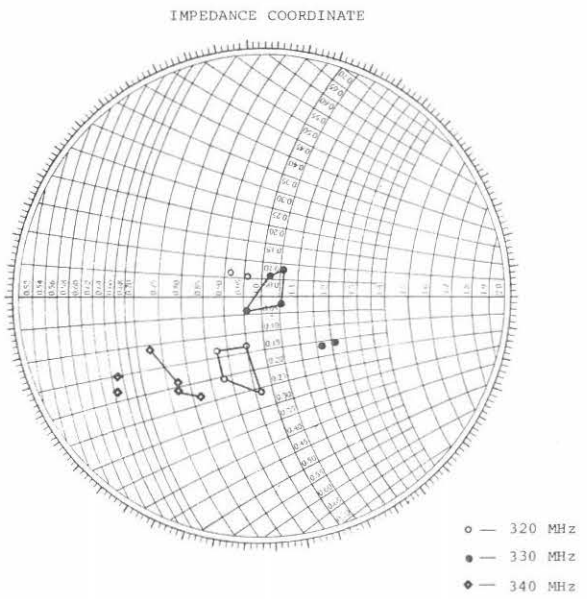

Fig. 10. The active impedance of the 6-element dipole array.

The active impedance of 6-element array was measured with a network-analyser and a 3 db-coupler inserted between a matching section and a power divider as shown in Figure 9. One of the 6 outputs of the power divider is adjusted so that its phase and amplitude are equal to those of other outputs when it is supplied to a dipole through the 3 db-coupler. The impedance-matching circuit was adjusted at a frequency of 327 MHz and the impedance measurements were made at frequencies of 320, 330 and 340 MHz. Results are shown on the Smith chart (Figure 10). A group of four points connected with lines on the chart represents the impedances of four dipoles except for the two at the both edges. Since a dipole at the edge cannot be regarded as one of uniformly spaced dipoles, its impedance differs from others due to the edge effect. As the impedances of the four dipoles scatter in small region on the chart, the impedances measured for the inner dipoles of the 6-element array can be considered to contain little edge effect and to be equal to the impedance for the array of more than 6 elements.

4. The receiver

Block and level diagrams of RF and IF sections are shown in Figures 11 and 12. The center frequency of the receiving band is 327 MHz and the IF frequency is 70 MHz. The system bandwidth is 2.5 MHz and this bandwidth is limited by terrestrial interferences. This frequency-band centered at 327 MHz is not protected for radio astronomy in Japan but is seldom used.

At the front-end, phase-controlled signals from the 96 phase shifters are combined into four groups; the four signals are introduced into the receiver room by long coaxial cables (5D2W) after amplification by amplifiers A2 and A3; four signals from the front-end are combined after passing through the phase shifters and RF switches at the input of the back-end. The phase and gain of the front-end can be measured with these RF switches.

The system temperature including the galactic background (300°K) is about 660°K. Using a integration time of 0.15 sec and the bandwidth of 2.5 MHz, the minimum detectable flux is about 5 flux units (1 flux unit = 10^{-26} w/m^2/Hz) for the total power system.

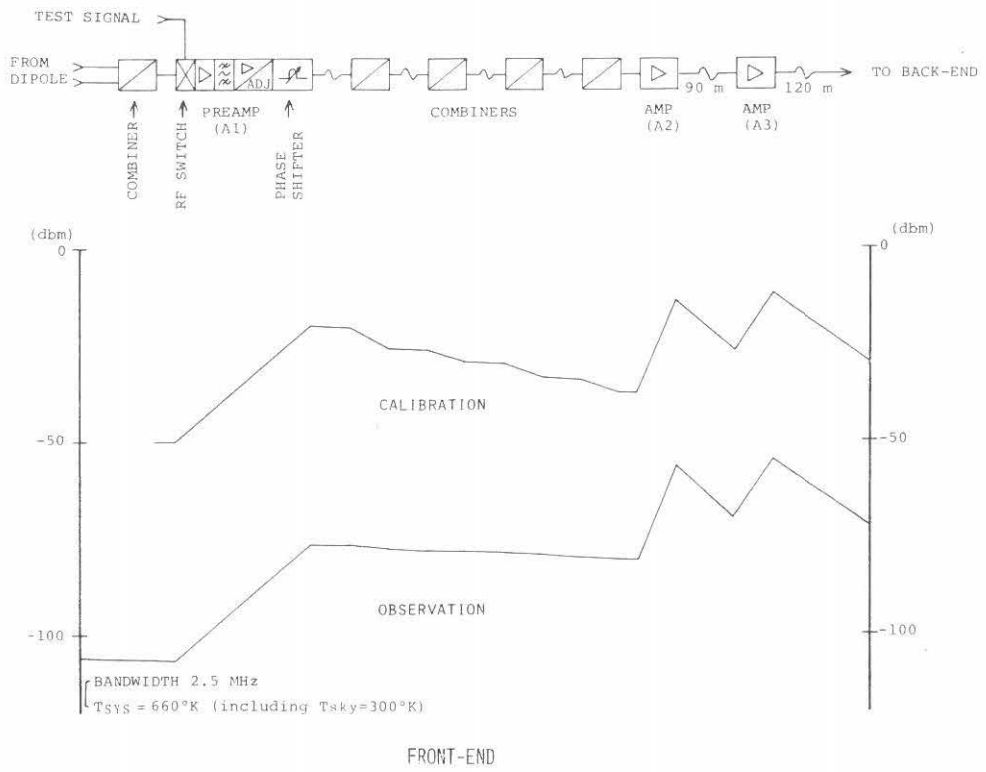

Fig. 11. Block diagram and level diagram for the system noise and the test signal at the front-end.

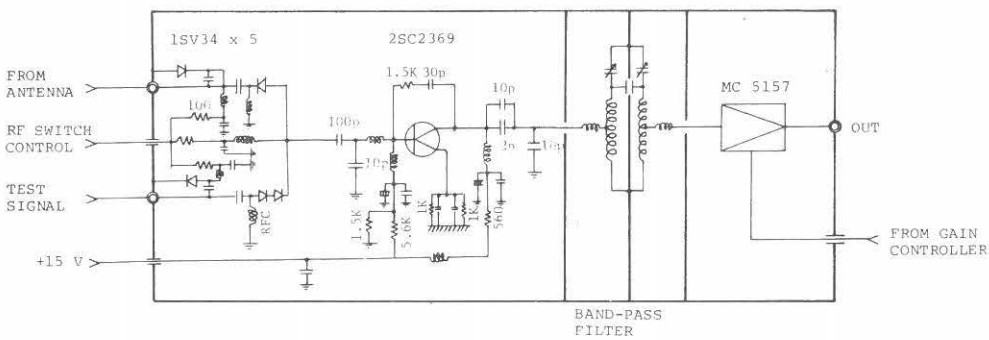

Fig. 13. Preamplifier.

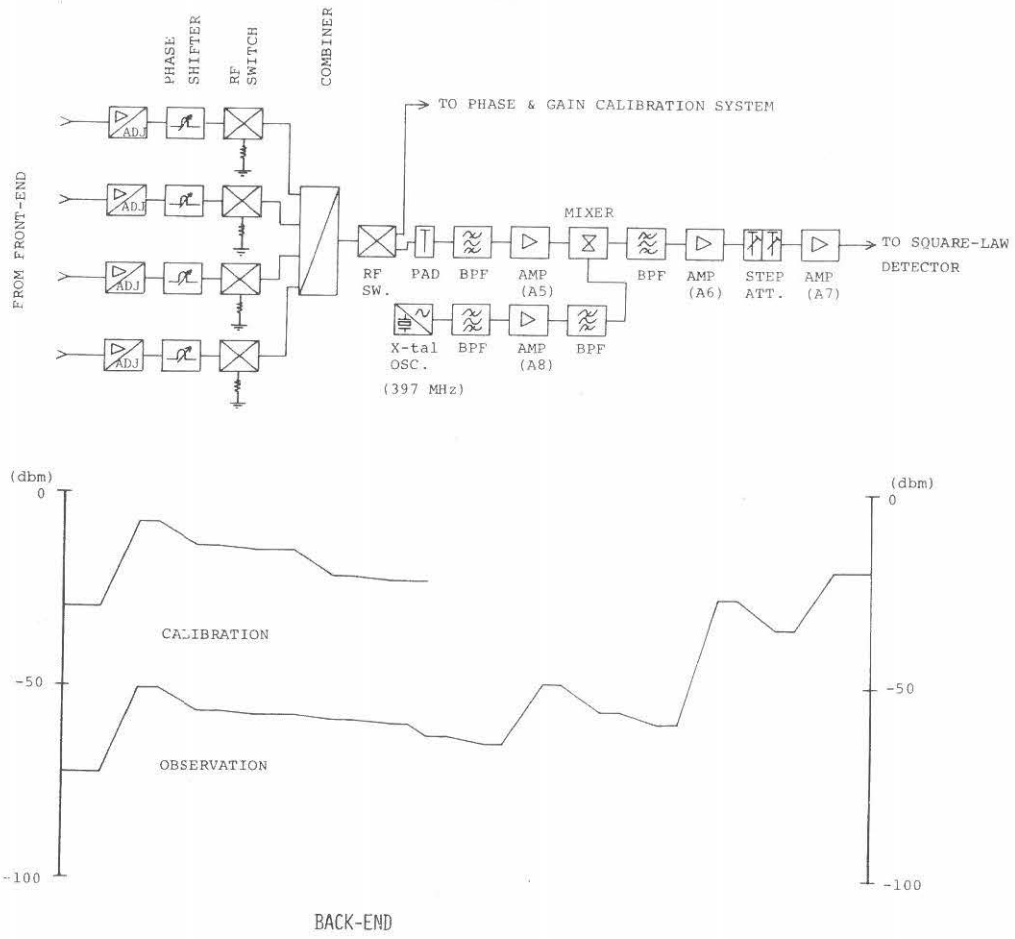

Fig. 12. Block diagram and level diagarm at the back-end.

4.1. The preamplifier

The preamplifier consists of two stages as shown in Figure 13. The first stage is a low-noise amplifier with a PIN-diode switch at the input which selects either the signal from the antenna or the test signal. Typical value of noise figure is 2.8 db including insertion loss of the PIN-diode switch. The second stage is a wide-band amplifier constructed with a hybrid IC (MC5157) whose gain can be varied by changing the supply DC voltage. This is used for the gain control of the system calibration. The RF band-pass filter is inserted between two amplifiers for protection against cross modulation due to terrestrial noises.

4.2. The phase shifter

The phase shifter is a ladder type and the steps are arranged in a binary fashion with a variation of 0° to 511° as shown in Figure 14. Small phase shift is given by a strip line and large shift is given a semirigid cable. Phase switches are constructed with PIN-diodes mounted on a printed circuit board. DC current to PIN-diodes is supplied through latch type relays, which are used for the purpose of data memory and protection against interferences such as radio noise from lightning. Insertion loss of direct and delay paths is carefully adjusted to be equal each other by adding small attenuation to a direct path. When the phase shifter is controlled from 0° to 511° at 1° steps, variation of the insertion loss is typically 0.16 db (rms) and phase error is typically 1.1 degrees (rms).

Phase shifters are controlled as shown in Figure 15. The phase data are given to terminals D1 to D9 and phase shifts are produced by the phase shifter when +5 V is applied to its LOAD terminal. Control speed for one phase shifter is as fast as 1 msec, and it takes 96 msec to control all of 96 phase shifters in series. It is desired that phase shifter control finishes within a data sampling interval of 50 msec; therefore, 96 phase shifters are divided into 12 groups of 8 phase shifters; the eight phase shifters in each group are controlled in series but 12 groups are controlled in parallel to reduce the control time.

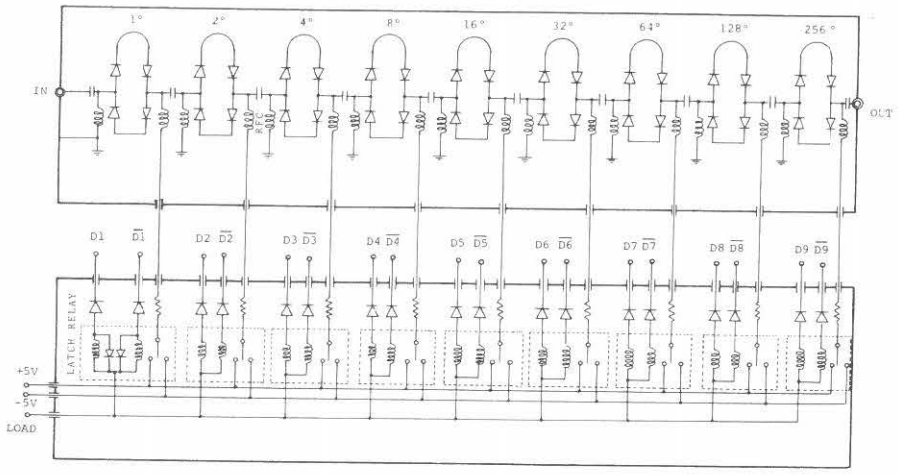

Fig. 14. Phase shifter. Dl to D9 are data inputs. When +5 V is supplied to LOAD terminal, phase shifts are produced.

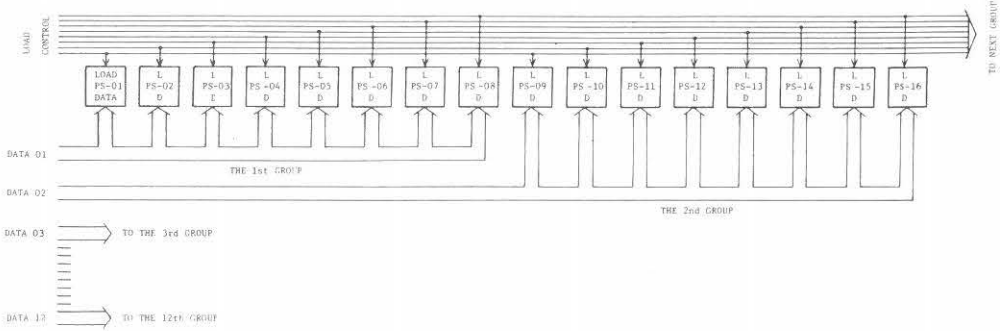

Fig. 15. Eight phase shifters are grouped and controlled in series. There are 12 groups which are controlled in parallel.

4.3. The LF section

A block diagram of the LF section is shown in Figure 16. The LF signal output from the square-law-detector is amplified; the DC component due to the receiver and galactic background noises, which is about 100 times as large as scintillating component, is removed by a high-pass filter (f_c = 0.04 Hz); the output of the high-pass filter is digitized with a 10-bit A/D converter.

When phase shifters are controlled to track a radio source, small system-gain-change occurs due to phase errors and/or variation of insertion loss of phase shifters. This small gain-change produces a sudden jump of the DC level at the input of the high-pass filter. A sudden jump of even as little as -20 db produces large disturbance, which lasts more than 10 sec, at the output of the high-pass filter. As the phase shifters are controlled every several tens of seconds, this long lasting disturbance is serious. To remove this undesirable disturbance, the cutoff frequency of the filter is changed from 0.04 to 30 Hz when phase shifters are controlled. The gain-change is also suppressed with an automatic-gain-control circuit as shown in Figure 17. This AGC works at the instant of controlling the phase shifters. A multiplier is used for the gain controller. DC voltage for gain control is supplied by an analog memory. When a control signal to terminal A in Figure 17 is of a high level, this memory functions as a voltage follower and then the AGC feed-back loop is closed. When a control signal returns to a low level, the AGC loop is opened and the gain of the multiplier is fixed.

5. The calibration system

As the antenna beam is formed and steered in the E-W direction with the phased array, phase and gain of each element of the array must be adjusted properly. Otherwise a system-gain-loss and a tracking error of a radio source will occur. The caribration of the system-gain is especially important in order to measure the scintillation index, from which we can derive the degree of the solar wind electron density fluctuation.

The calibration of phase and gain is performed by feeding the

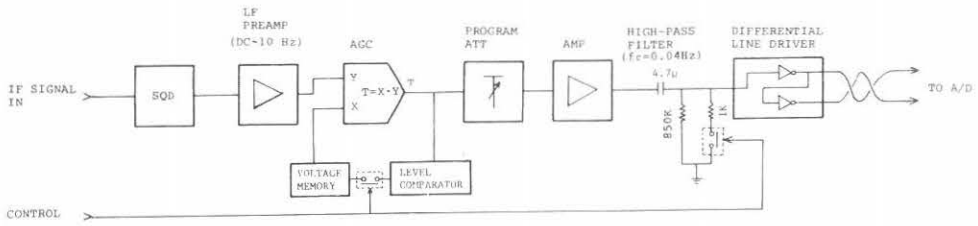

Fig. 16. Block diagram of the LF section. When the switch of AGC is closed, the voltage memory functions as a voltage follower.

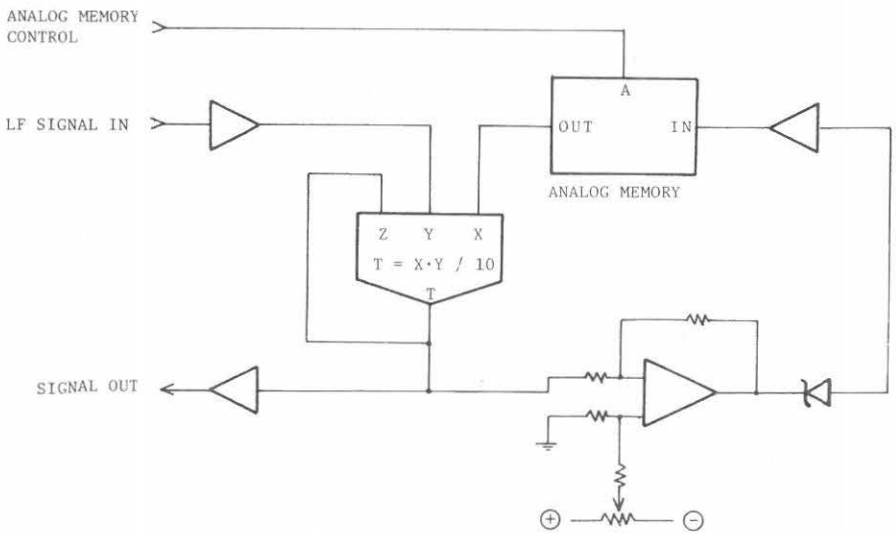

Fig. 17. Automatic-gain-control circuit used at the LF section. When the terminal A of the analog memory is high level, the analog memory functions as a voltage follower. When A is low level, the output is isolated from the input and the DC voltage is memorized.

test signal to the preamplifiers and by comparing the phase and amplitude of output signals from two adjoining channels. The branching system of the test signal is shown in Figure 6. The test signal from the signal generator is distributed into 96 branches; at each branch, the test signal out of a RF amplifier, which functions as an isolator and a RF switch, is divided in two; these divided signals are supplied to adjoining two preamplifiers.

This method is independent of differences in electrical conditions among the branches. As a calibration error arises when there is leakage of the test signal to other channels, the leakage is carefully protected with isolation amplifiers, padding attenuators and hybrid combiners whose inputs are highly isolated from each other as shown in Figure 18.

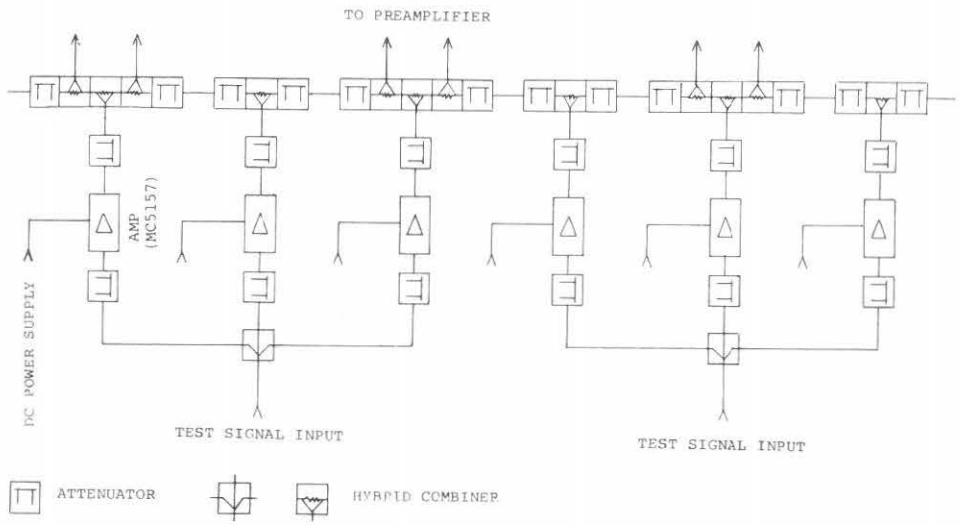

Fig. 18. Branching system of test signal. To select a branch, DC power is supplied to MC5157 of its branch. Outputs of the MC5157 are supplied to the adjoining preamplifiers.

The demerit of this calibration method is the fact that the experimental errors are accumulated, because the phase and gain of each channel are not obtained directly but indirectly by repeating phase (or gain) comparison between adjoining channels successively. However, this error can be reduced by taking many measurements and using their average values in calibration. This is achieved by the ability of high speed calibration. This calibration system is now under adjustment, but there is no problem in the gain control and phase measurement at high speed. The calibrations are performed automatically with a microprocessor (Figure 20) and the processing speed of this processor will decide the calibration speed.

5.1. The gain calibration

The gain of the first preamplifier is calibrated absolutely with the noise generator; the other 95 preamplifiers are calibrated relatively with the test signal from the signal generator so that gains of adjoining amplifiers are equal each other. The gain control is performed by the hybrid IC (MC5157) in the preamplifier (Figure 13). DC voltage to control the gain of IC is supplied by the adjustable voltage regulator whose feed-back resistors are controlled by the circuit shown in Figure 19. The gate of the clock pulse is opened to begin the gain control; the feed-back resistors change according to the count of the clock pulse; when the gain becomes equal to that of the adjoining channel, the gate is closed. The number of the count is memorized in the microprocessor; this process of the gain adjustment is repeated and the average value of the counts is calculated for each channel; finally, the average count is loaded to each counter through PRESET terminals.

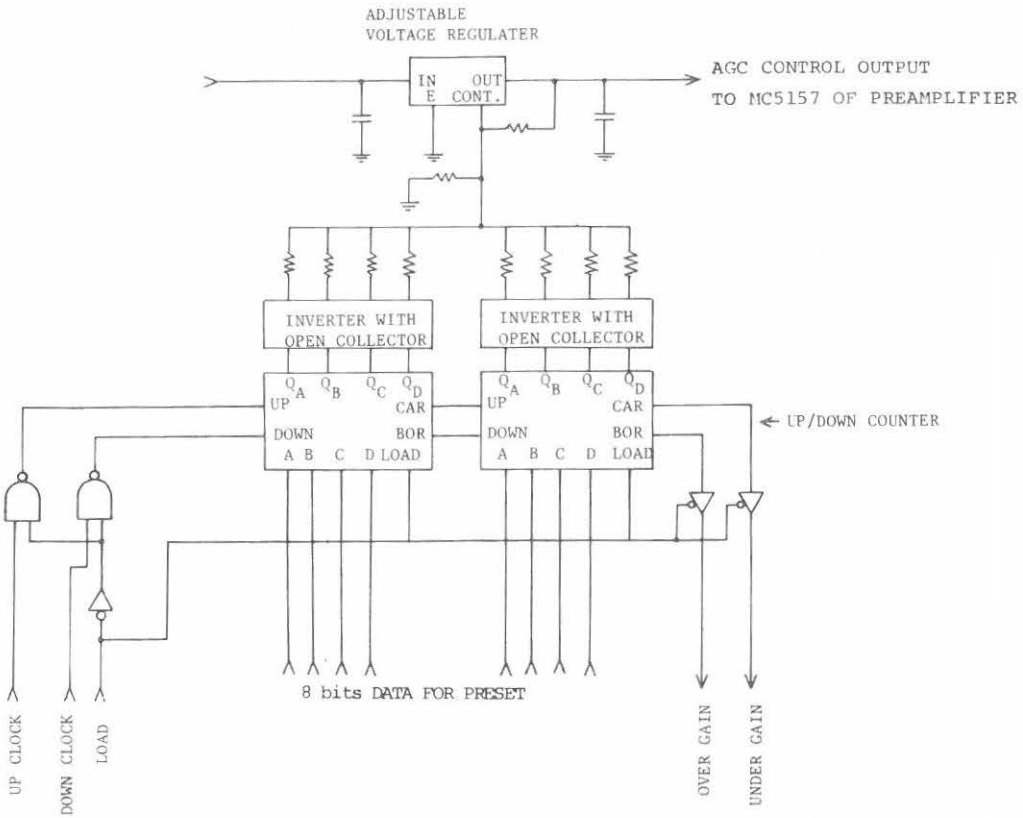

Fig. 19. Output of the adjustable voltage regulator controls the gain of the preamplifier. Feed-back resistors change according to up/down counting.

5.2. The phase calibration

The phase calibration is made after the gain calibration, because the phase characteristics of MC5157 changes by adjusting its gain. The calibration system measures the phase of the test signal passing through the front-end and calculates the phase offset of each channel relative to the first channel. The results of the calculation are sent

to the observation control system. The phase offsets are corrected when the phase shifters are controlled.

6. The observation control system

The observation control system is shown in Figure 20. The main constituent is a microprocessor: The program timer produces timing signals for the system control with the clock signal from the "time standard": The "time standard" which is also used in the VHF observation system (Kojima et al., 1979) assures time coincidence among the stations within a few msec. Main tasks of this control system are

(1) the calculation of the coordinates of a radio source,
(2) the control of the antenna in the N-S direction,
(3) the control of the phase shifters to track a radio source correcting the phase offsets measured by the calibration system,
(4) the control of the receiver gain, and
(5) monitoring conditions of the observation system: power trouble, temperature, antenna trouble, etc..

The microprocessor calculates the parameters necessary for the next observation: the time interval of the antenna beam control, the observation start time, the duration of the observation, the elevation angle of the antenna, phase data, etc.. These parameters are provided to the program timer, the phase-shifter controller and the antenna controller. The three parameters of the time interval for the beam control, the start time and the duration of the observation are programed in the timer by the microprocessor. The timer produces the interruption signal for the microprocessor periodically to control the phase shifters and the antenna elevation angle; when the microprocessor accepts this signal, it sends the phase data to the phase-shifter controller and the elevation angle to the antenna controller; the processor begins calculation of the parameters for the next step. The timer also produces control signals for the A/D converter. The antenna controller controls the antenna elevation angle by comparing the data from the processor and the output of the shaft encorder; the antenna controller also monitors the antenna troubles and produces the interruption signal to the processor when trouble

occurs. The observation control system is connected to the calibration system with a data line between two microprocessors and can obtain the results of the phase measurements.

To do these many tasks, the interruption level of the processor is increased by as many as 24 levels. The processor is normally in the state of "hold" and begins processing these tasks when it accepts interruption signals.

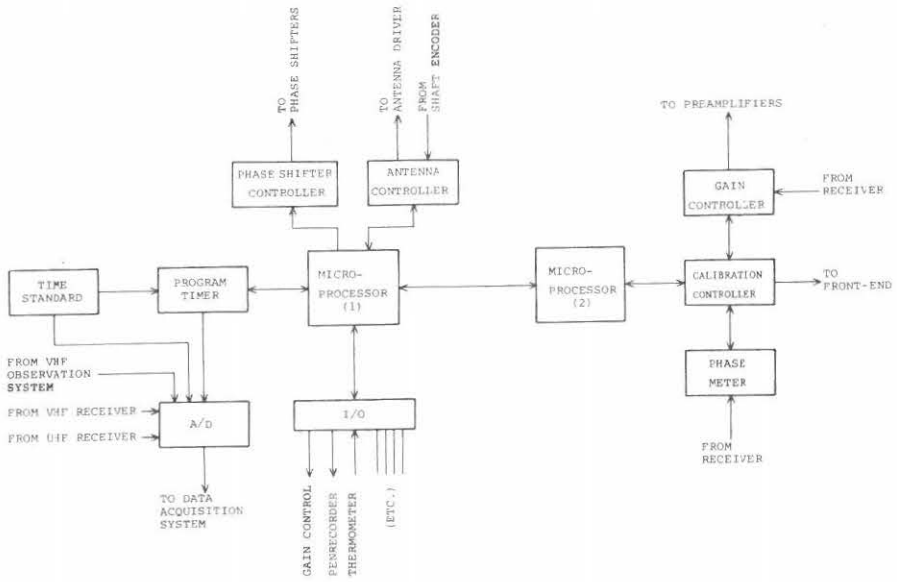

Fig. 20. Block diagram of the observation control system and the calibration system

7. The data acquisition system

A block diagram of the data acquisition system is shown in Figure 21. At the host station, data acquisition is controlled by the minicomputer MS 30 (NEC) which is the subsystem of the host computer ACOS 700 (NEC). At the each remote station, minicomputer OKITAC 4300 is used; data are stored on a magnetic tape and transmitted to the host station during off-observation time by the public telephone lines at a speed of 1200 baud. The transmitted data and the data obtained at the host station are stored temporarily in a magnetic disc, and transmitted to the host computer at a speed of 48 kilobaud for data analysis and permanent preservation of data. The magnetic tapes at the remote stations can be erased and initialized by a command from the host station. All of the data acquisition is controlled automatically by the scheduler of MS 30.

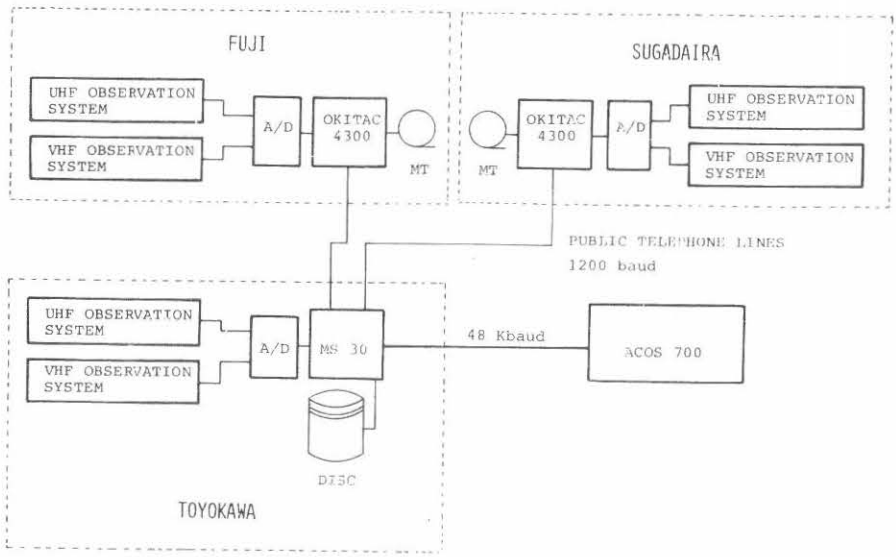

Fig. 21. Data acquisition system

Acknowledgements

We wish to express our gratitude to Dr. G. Swarup for providing valuable data about the corner reflector and the phase shifter. We are also thankful to Dr. G.J. Nelson for his valuable discussion about our observation system. At Sugadaira, the antennas of VHF and UHF are placed in Sugadaira Space Radio Wave Observatory, University of Electro-Communications, through the courtesy of Prof. T. Yoshino and his colleagues. Part of this work has been supported by the Grant in Aid for Scientific Research of the Ministry of Education, Culture, and Science (542004).

References

Braccesi, A. and Ceccarelli, A.: The Italian Cross Radiotelescope. I - Design of the antenna, Nuovo Cimento 23, 208 (1962).

Gapper, G.R. and Hewish, A.: Density Gradient in the Solar Plasma Observed by Interplanetary Scintillation, Mon. Not. R. astr. Soc., 197, 209 (1981).

Kojima, M., Watanabe, T., Ishida, Y., Maruyama, K., and Kakinuma, T.: A Full-Automatic System for the Observations of Interplanetary Scintillation, Proc. Res. Inst. Atmospherics, Nagoya Univ., 26, 95 (1979).

Swarup, G., Sarma, N.V.G., Joshi, M.N., Kapahi, V.K., Bagri, D.S., Damle, S.H., Ananthakrishnan, S., Balasubramanian, V., Bhave, S.S., and Sinha, R.P.: Large Steerable Radio Telescope at Ootacamund, India, Nature Phys. Science, 230,185 (1971).